MOLECULAR IMAGING AND BIOLOGY

Mol Imaging Biol (2017) 20:605–614
DOI: 10.1007/s11307-017-1153-z

Published Online: 2 January 2018

RESEARCH ARTICLE

Astroglial Responses to Amyloid-Beta Progression in a Mouse Model of Alzheimer's Disease

Malin Olsen,[1] Ximena Aguilar,[1] Dag Sehlin,[1] Xiaotian T. Fang,[1] Gunnar Antoni,[2,3] Anna Erlandsson,[1] Stina Syvänen[1]

[1]*Department of Public Health and Caring Sciences/Geriatrics, Rudbeck Laboratory, Uppsala University, Dag Hammarskjölds väg 20, SE-751 85, Uppsala, Sweden*

[2]*Department of Medicinal Chemistry, Preclinical PET Platform, Uppsala University, Dag Hammarskjölds väg 20, SE-751 83, Uppsala, Sweden*

[3]*PET Centre, Uppsala University Hospital, Entrance 70, Sjukhusvägen 10, SE-75185, Uppsala, Sweden*

Abstract

Purpose: Alzheimer's disease (AD) is a neurodegenerative disorder characterized by amyloid-beta (Aβ) deposition, hyperphosphorylation of tau, and neuroinflammation. Astrocytes, the most abundant glial cell type in the nervous system, respond to neurodegenerative disorders through astrogliosis, *i.e.*, converting to a reactive inflammatory state. The aim of this study was to investigate how *in vivo* quantification of astrogliosis using positron emission tomography (PET) radioligand deuterium-L-[^{11}C]deprenyl ([^{11}C]DED), binding to enzyme monoamine oxidase-B (MAO-B) which is overexpressed in reactive astrocytes during AD, corresponds to expression of glial fibrillary acidic protein (GFAP) and vimentin, *i.e.*, two well-established markers of astrogliosis, during Aβ pathology progression.

Procedures: APP_{ArcSwe} mice ($n = 37$) and wild-type (WT) control mice ($n = 23$), 2–16-month old, were used to investigate biomarkers of astrogliosis. The radioligand, [^{11}C]DED, was used as an *in vivo* marker while GFAP, vimentin, and MAO-B were used to investigate astrogliosis and macrophage-associated lectin (Mac-2) to investigate microglia/macrophage activation by immunohistochemistry of the mouse brain. Aβ and GFAP levels were also measured with ELISA in brain homogenates.

Results: The intrabrain levels of aggregated Aβ and reactive astrocytes were found to be elevated in APP_{ArcSwe} compared with WT mice. GFAP and vimentin expression increased with age, *i.e.*, with Aβ pathology, in the APP_{ArcSwe} mice. This was not the case for *in vivo* marker [^{11}C]DED that showed elevated binding of the same magnitude in APP_{ArcSwe} mice compared with WT mice at both 8 and 16 months. Further, immunohistochemistry indicated that there was limited co-expression of MAO-B and GFAP.

Conclusions: MAO-B levels are increased early in Aβ pathology progression, while GFAP and vimentin appear to increase later, most likely as a consequence of abundant Aβ plaque formation. Thus, [^{11}C]DED is a useful PET radioligand for the detection of changes in MAO-B at an early stage of

Electronic supplementary material The online version of this article (https://doi.org/10.1007/s11307-017-1153-z) contains supplementary material, which is available to authorized users.

Correspondence to: Stina Syvänen; *e-mail:* stina.syvanen@pubcare.uu.se

AD progression but does not measure the total extent of astrogliosis at advanced stages of Aβ pathology.

Key words: PET, Amyloid-beta, Astrocytes, Astrogliosis, MAO-B, GFAP, Vimentin, [^{11}C]DED

Introduction

Alzheimer's disease (AD) is the most common form of dementia and estimated to affect around 50 million people worldwide. The pathophysiology of AD is complex and involves cellular processes, such as amyloid beta (Aβ) deposition into amyloid plaques, hyperphosphorylation of tau, and aggregation of tau into neurofibrillary tangles, oxidative stress, apoptosis, and neuroinflammation.

According to the amyloid cascade hypothesis, mis-metabolism of Aβ is the first event in AD development and all other neuropathological features of AD are secondary events, induced by the Aβ pathology [1]. Monomeric Aβ is very prone to aggregate into smaller and larger soluble Aβ assemblies, which can then further aggregate into insoluble fibrils, which eventually deposit as Aβ plaques. Originally plaques were considered to be neurotoxic to neurons, but several studies indicate that soluble Aβ aggregates, *e.g.*, oligomers and protofibrils, are the toxic forms of Aβ and that these smaller aggregates are capable of inducing neuronal death [2–7].

It is debated whether the inflammatory changes occurring in the brain during AD are caused by or are causing the pathology. Neuroinflammation has beneficial roles, *i.e.*, by inducing phagocytosis of apoptotic cells and debris and by inducing tissue repair processes with the primary goal of protecting the CNS from injury and diseases. However, inflammatory activities that are proceeding uninhibited can cause cellular dysfunction and may eventually be contributing to the pathophysiology of AD [8]. For example, it is known that the expression of pro-inflammatory molecules, such as IL-1, IL-6, and TNF-α, is altered in an AD brain [9].

Astrocytes are the most abundant glial cell type. Until quite recently, the function of astrocytes was believed to be a structural support for the neuronal network. However, it has now become clear that astrocytes are responsible for a variety of important functions in the brain including metabolic support of neurons, modification of synapse signaling, recycling of neurotransmitters, blood-brain barrier regulation, and glymphatic clearance [10–12].

Reactive astrogliosis is a process in which astrocytes convert to an inflammatory state. This process is triggered by some type of pathological condition in the micro-environment surrounding the astrocytes, *e.g.*, the presence of mis-folded proteins [13]. For example, reactive astrocytes are together with microglia found in the close proximity to Aβ plaques [14, 15]. The tightly packed glial cells might protect the surrounding brain tissue from the plaque itself and from toxic, soluble Aβ species that might appear at the plaque site. However, the glial cells play a rather complex role during the disease process and are known to secrete cytokines and other factors that could be either neurotoxic or neuroprotective [16]. For example, an increased expression of pro-inflammatory molecules can stimulate γ-secretase activity and enhance the processing of APP, potentially leading to an exacerbation of the Aβ pathology [17].

Reactive astrocytes are phagocytic cells that are able to ingest dead cells, neuronal synapses, and protein aggregates of Aβ and α-synuclein [18–22]. Especially in early stages of AD, astrocytes appear to be even more efficient than microglia in engulfing Aβ [22]. However, their exact role in the pathophysiology is not well understood [8]. One of the hallmarks of astrogliosis is the increased expression of the intermediate filament proteins glial fibrillary acidic protein (GFAP) and vimentin.

L-Deprenyl is an irreversible inhibitor of the enzyme monoamine oxidase B (MAO-B). MAO-B is found on the outer membrane of the mitochondria, predominately in astrocytes in the brain [23]. The positron emission tomography (PET) radioligand deuterium-L-[^{11}C]deprenyl ([^{11}C]DED) displays high specificity and affinity for MAO-B [24]. The enzyme is overexpressed in reactive astrocytes, such as those for example in AD. Several clinical PET studies have thus suggested that [^{11}C]DED can be used as a PET ligand for measuring the MAO-B activity in AD brains as an *in vivo* marker for early disease progression [25–29].

There are currently two standpoints on whether astrogliosis is preceding the plaque pathology or if the plaque pathology is initiating the astrogliosis. Based on recent studies with [^{11}C]DED PET imaging of astrogliosis it has been suggested that astrogliosis occurs early in AD and precedes the occurrence of insoluble plaques [30], while other studies have found an increase of astrogliosis in parallel with the progression in Braak stages [31]. The aim of this study was to investigate how *in vivo* quantification of astrogliosis using PET radioligand [^{11}C]DED corresponds to the amount of reactive astrocytes found in different brain regions using GFAP and vimentin immunohistochemistry, and GFAP ELISA in isolated brain tissue from young and old APP_{ArcSwe} and wild-type control (WT) mice.

Methods

Animals

Male (n = 21) and female (n = 16) APP_{ArcSwe} mice, obtained by in-house breeding on a C57bl/6 background, and non-

transgenic male (n = 10) and female (n = 13) WT littermates of the same age were used. APP_{ArcSwe} mice show elevated levels of soluble Aβ aggregates already at a very young age and a developing plaque pathology starting at around 6–7 months of age [32, 33]. Aβ pathology first appears as intraneuronal inclusions in the cerebral cortex and hippocampus and later as larger extracellular assemblies. Pathology then spreads to thalamus and striatum. Opposite to many other mouse models of Aβ pathology, APP_{ArcSwe} mice display dense-cored plaques resembling those found in human AD brains. The mice were housed at an animal facility at Uppsala University at 20–22 °C, with access to food and water *ad libitum* on a 12-h light/dark cycle. At the time of euthanisation, mice were deeply anesthetized with 2.7–3.2 % isoflurane (Baxter Medical AB, Kista, Sweden) followed by intracardiac perfusion with 50 ml physiological saline during 2 min. After perfusion, the brain was removed from the cranium and divided by the midline into two pieces. The left hemisphere was snap frozen on dry ice to be used for biochemical quantification of Aβ and GFAP. The right hemisphere was placed in paraformaldehyde for 24 h. After 24 h, it was cryoprotected in sucrose (10, 20, and finally 30 %) and stored in 30 % sucrose at 4 °C until cryosectioned for immunohistochemical analysis. The cerebellum, which is largely devoid of Aβ pathology [34], was removed before homogenization of the left hemisphere. Details are provided in Electronic Supplementary Material (ESM).

PET Scanning

The PET radioligand [^{11}C]DED was synthesized as previously described [35]. Four groups of animals were investigated; 8-month-old APP_{ArcSwe} (n = 5), 8-month-old WT (n = 5), 16-month-old APP_{ArcSwe} (n = 4), and 16-month-old WT (n = 6). Animals were anesthetized with isoflurane and the tail vein was cannulated for [^{11}C]DED administration. The animal was then immediately placed in a prone position on a pre-heated bed in the gantry of the PET/CT scanner (intrinsic resolution 1.35 mm, Triumph Trimodality System, TriFoil Imaging, Inc., Northridge, CA, USA). Anesthesia was maintained throughout the study using 1.5–2.0 % isoflurane in a 0.5-l/min flow of 50 % oxygen and 50 % medical air. [^{11}C]DED, 11.1 ± 4.2 MBq (5.8 ± 8.9 GBq/μmol) in 120 μl, was injected *via* the tail vein at the start of the PET scan. The acquisition time in the PET scanner was 30 min, followed by a CT examination for 3 min with a field of view (FOV) of 8 cm. A terminal blood sample from the heart was obtained 60 min after injection of the radioligand. The brain was then isolated as described above. Radioactivity in the blood and the frozen brain samples was measured with a γ-counter (1480 WizardTM, Wallac Oy, Turku, Finland).

A MLEM 2D algorithm (ten iterations) and filtered back projection (FBP) was used to reconstruct the PET data and the CT raw files, respectively. The PET image matrix size was 160 × 160 × 128 with a voxel size of 0.5 × 0.5 × 0.59 mm^3. Imaging software Amide 1.0.4 [36] was used to manually align the PET and CT images according to a previously described process [34]. In short, a MRI-based mouse brain atlas [37] was first aligned with the CT. This atlas contained outlined regions of interest for hippocampus, striatum, thalamus, cerebral cortex and cerebellum. The PET images were then aligned with the CT, and the regions of interest outlined in the MRI-atlas were transferred to the PET images. Binding potential (BP_{nd}) using time-activity curves from the whole scan time of 30 min was obtained in hippocampus, striatum, thalamus, and cerebral cortex using the simplified reference tissue model (SRTM) [38] with the cerebellum as reference region in Pmod (PMOD Technologies Ltd., Zürich, Switzerland). The cerebral cortex region did not include the prefrontal cortex as the measured activity in this part was confounded by spill-over from a hot-spot frontal to the brain (see results section).

Immunohistochemistry

Immunohistochemistry was performed to evaluate the expression of $Aβ_{1–42}$, GFAP, Vimentin, macrophage-associated lectin (Mac-2) and MAO-B in mice aged 8, 12, and 16 months (n = 4 $APP_{Arc-Swe}$, n = 2 WT for each age group). The brains were collected as described above and were cryosectioned (HM500, Microm GmbH, Walldorf, Germany) in 20-μm-thick sagittal sections ($n \geq 4$ sections per mouse). All steps were performed at room temperature (RT) unless mentioned otherwise. Detailed protocols are provided in the ESM.

Biochemical Analysis of GFAP and Aβ Pathology

To further analyze the protein concentration of GFAP in APP_{ArcSwe} mice in relation to disease progression, a sandwich ELISA was performed in brain homogenates (lysates) obtained from mice aged 2, 4, 6, 8, 12, and 16 months (n = 4 $APP_{Arc-Swe}$, n = 2 WT for each age group). A detailed protocol is provided in the ESM. Levels of Aβ40, corresponding to total plaque load, was measured in the formic acid treated brain homogenates. The ELISA was performed as previously described [34]. In addition to Aβ40, soluble Aβ protofibril levels in brain TBS homogenates was measured as previously described [34, 39]. Aβ concentrations were determined from a standard curve of serially diluted synthetic Aβ40 and Aβ protofibrils respectively. Both Aβ40 and Aβ protofibril levels were studied in the same groups of mice aged 4, 8, 12, and 16 months (n = 5 $APP_{Arc-Swe}$, n = 5 WT for each age group).

Statistics

The data was analyzed with two-way (PET BP_{ND}) or one-way (ELISA measured concentrations) ANOVA, using

Bonferroni's *post hoc* test. All data were analyzed in GraphPad Prism (version 6.07). The data are reported as mean ± standard deviation (SD). Significance levels, after Bonferroni correction, were labeled as *p value < 0.05), **p value < 0.01), and ***p value < 0.001).

Results

PET Scanning

The PET radioliagnd [^{11}C]DED was rapidly and abundantly distributed to the brain in both APP_{ArcSwe} and WT mice. The wash-out from the brain was also fast with intrabrain concentrations stabilizing around 10 min post-injection. PET images also revealed a very high radioligand concentration in a region, probably the Harderian gland, frontal to the brain (Fig. 1). Thus, BP_{ND} values based on the whole cortex were regarded as confounded by spill-over from this hot spot. Instead, a cortex region without the prefrontal part was used for analysis. *Ex vivo* measured radioactivity in isolated blood and whole brain samples at 60 min after administration of [^{11}C]DED was used to calculate a brain-to-blood concentration ratio. This ratio was 1.1 ± 0.2 (APP_{ArcSwe} 16 months), 1.1 ± 0.5 (WT 16 months), 1.1 ± 0.1 (APP_{ArcSwe} 8 months), and 1.0 ± 0.2 (WT 8 months).

BP_{ND} values are shown in Fig. 2. *Post hoc* analysis revealed that 16-month-old APP_{ArcSwe} mice displayed significantly higher BP_{ND} (2.3-fold) in the thalamus compared with 16-month-old WT mice (p = 0.016). Although this genotype-dependent trend was also observed in the other studied regions, it was not significant probably due to a rather large intragroup variation (p = 0.13 in hippocampus, p = 0.53 in striatum, p = 0.11 in cortex). Age was not found to have a significant impact on BP_{ND}, although there was a small trend towards higher values in 16-month-old APP_{ArcSwe} mice compared with 8-month-old APP_{ArcSwe} mice, while the opposite was found for WT mice, *i.e.*, younger WT mice displayed higher BP_{ND} than old WT mice.

Immunohistochemistry

Aβ, GFAP, and Mac-2

Distinct plaque formation in the brain was observed in the 8-month-old APP_{ArcSwe} mice, although some plaque pathology was found already in 6-month-old mice. The plaque formation was mainly seen in cortex, thalamus and hippocampus. In the 8-month APP_{ArcSwe} mice, a slight increase in GFAP-positive cells was found adjacent to the plaques in the cortex and hippocampus. In the 12-month APP_{ArcSwe} brains, a pronounced increase of GFAP-positive cells could be seen around the plaques in the same regions, with an additional expression in thalamus. In the brains of the 16-month-old APP_{ArcSwe} mice, GFAP-positive cells were found densely in the cortex, hippocampus, and thalamus, not only surrounding the plaques (Figs. 3 and 4). Astrocytes with a lower GFAP expression were also distributed in various regions of the brain.

When plaque formation was observed, Mac-2-positive cells, *i.e.*, activated microglia/macrophages, were found surrounding the Aβ deposits in the cortex, hippocampus, and thalamus (Fig. 3). It was difficult to distinguish separate Mac-2-positive cells from each other as they were clustered together. Interestingly, a few cells at all ages were double positive for GFAP and Mac-2.

Brains isolated from young APP_{ArcSwe} mice with no plaque pathology displayed a comparable expression pattern of astrocytes and microglia as brains from WT mice (Figs. 3 and 4). In these mice, the expression of GFAP was found to be relatively low, and the positive cells were predominantly found in regenerative areas, surrounding the lateral ventricle and in the hippocampus, indicating they were mainly neuronal precursor cells. Very few Mac-2-positive cells were found in wild-type mice and in the younger APP_{ArcSwe} mice with no visible plaque pathology.

Vimentin

To further investigate the astrocytic response to plaque formation, another reactive astrocytic marker, vimentin, was studied. A similar appearance of vimentin-positive cells to the GFAP-positive cells was seen, however, the expression pattern was slightly different from that of GFAP (Fig. 4). Vimentin was found to have an overall low expression in all regions of the brain at early ages. When plaque formation was observed in the 8-month-old APP_{ArcSwe} mice, the vimentin expression increased in the cortex, and in the 12-month-old APP_{ArcSwe} mice, the expression also increased in thalamus. The expression of vimentin in hippocampus remained quite low even in the older mice where plaque formation was observed. A main difference in the expression pattern between vimentin and GFAP was seen in the 16-month-old APP_{ArcSwe} mice, where vimentin-positive cells were only located distinctly around the plaques, while GFAP-positive cells were found throughout the brain. Many of the reactive astrocytes co-expressed GFAP and vimentin. Among the cells only expressing one of the markers, there were more single positive cells for GFAP than for vimentin. The expression of vimentin in the WT mice was very low and was only found in the hippocampus and surrounding the ventricles.

MAO-B

Expression of MAO-B was also investigated with immunohistochemistry in APP_{ArcSwe} and WT mice of different ages. However, no significant differences in expression levels

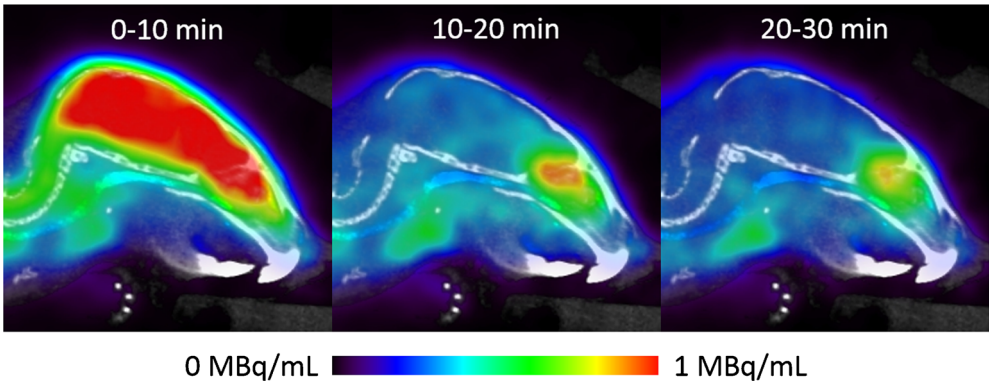

Fig. 1 [^{11}C]DED binding in the brain of 16-month-old APP_{ArcSwe} mouse. Sagittal PET/CT images averaged over 0–10, 10–20, and 20–30 min, respectively, after injection of 8 MBq [^{11}C]DED. After initial high and homogenous brain distribution, concentrations decreased with some longer retention times in midbrain and cortical regions. [^{11}C]DED also showed high uptake in a region frontal to the brain, most likely the Harderian glands.

between the different groups were observed. Interestingly, there was very little co-localization between MAO-B and GFAP (Fig. 5).

Biochemical Quantification of GFAP and Aβ Protofibrils

To further evaluate the expression pattern of astrocytic markers observed with immunohistochemistry, the expression of GFAP was studied in a sandwich ELISA. An optical density (OD) of GFAP was obtained from the ELISA. A significant difference was found between the 16-month-old APP_{ArcSwe} mice and the WT group ($p < 0.001$) and between the 12-month APP_{ArcSwe} mice and the WT group ($p < 0.01$). These old APP_{ArcSwe} mice also displayed significantly more GFAP than younger APP_{ArcSwe} mice (Fig. 6a) ($p < 0.001$ 16 months *vs.* 2 and 4 months, $p < 0.01$ for 16 months *vs.* 6 and 8 months, $p < 0.01$ for 12 months *vs.* 2 and 4 months). In line with the age-dependent increase in GFAP levels, both total Aβ40 and TBS-soluble Aβ protofibril levels increased with age in the APP_{ArcSwe} mice (Fig. 6b, c). For Aβ40, corresponding to total plaque load [32, 40], there was a large increase between 8 and 12 months.

Discussion

Neuroinflammation is a pathophysiologic event involved in AD where activation of astrocytes seems to be a key feature. The present study aimed at comparing *in vivo* PET and *ex vivo* markers for astrogliosis with levels of aggregated Aβ in APP_{ArcSwe} mice during pathology progression. The *in vivo* marker and PET radioligand [^{11}C]DED binding to MAO-B, which is overexpressed in reactive astrocytes, showed an increasing trend in APP_{ArcSwe} mice compared with WT. However, there was no difference in [^{11}C]DED binding between 8- and 16-month-old APP_{ArcSwe} mice, suggesting that MAO-B levels do not increase with further increasing amount of aggregated Aβ and potentially that elevated MAO-B levels are an early event during Aβ pathology progression. In fact, the major increase in Aβ deposition was found between 8 and 12 months, while MAO-B levels appeared to be elevated already at 8 months. These results are also in line with a previous study that

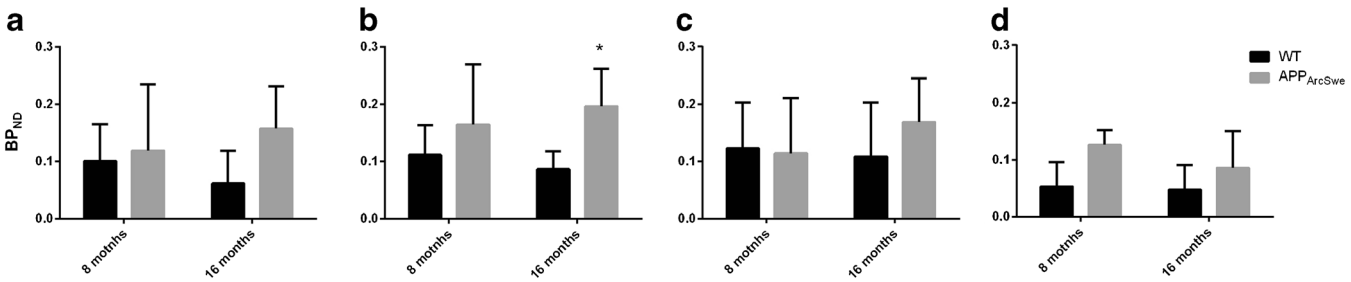

Fig. 2 Binding of [^{11}C]DED in brain of APP_{ArcSwe} and WT mice. Binding potential (BP_{ND}, 0–30 min) using SRTM in **a** hippocampus, **b** thalamus, **c** striatum and **d** cerebral cortex. The frontal parts of cerebral cortex region was omitted from the analysis due to spill-over from a hot spot frontal to the brain. There was a trend indicating that BP_{ND} was elevated in APP_{ArcSwe} mice compared with WT mice. The difference between WT and APP_{ArcSwe} was only significant in 16-month-old mice in the region of thalamus. ($n = 5$ in 8-month-old WT and APP_{ArcSwe} groups, $n = 6$ in 16-month-old WT group, and $n = 4$ in 16-month-old APP_{ArcSwe} group).

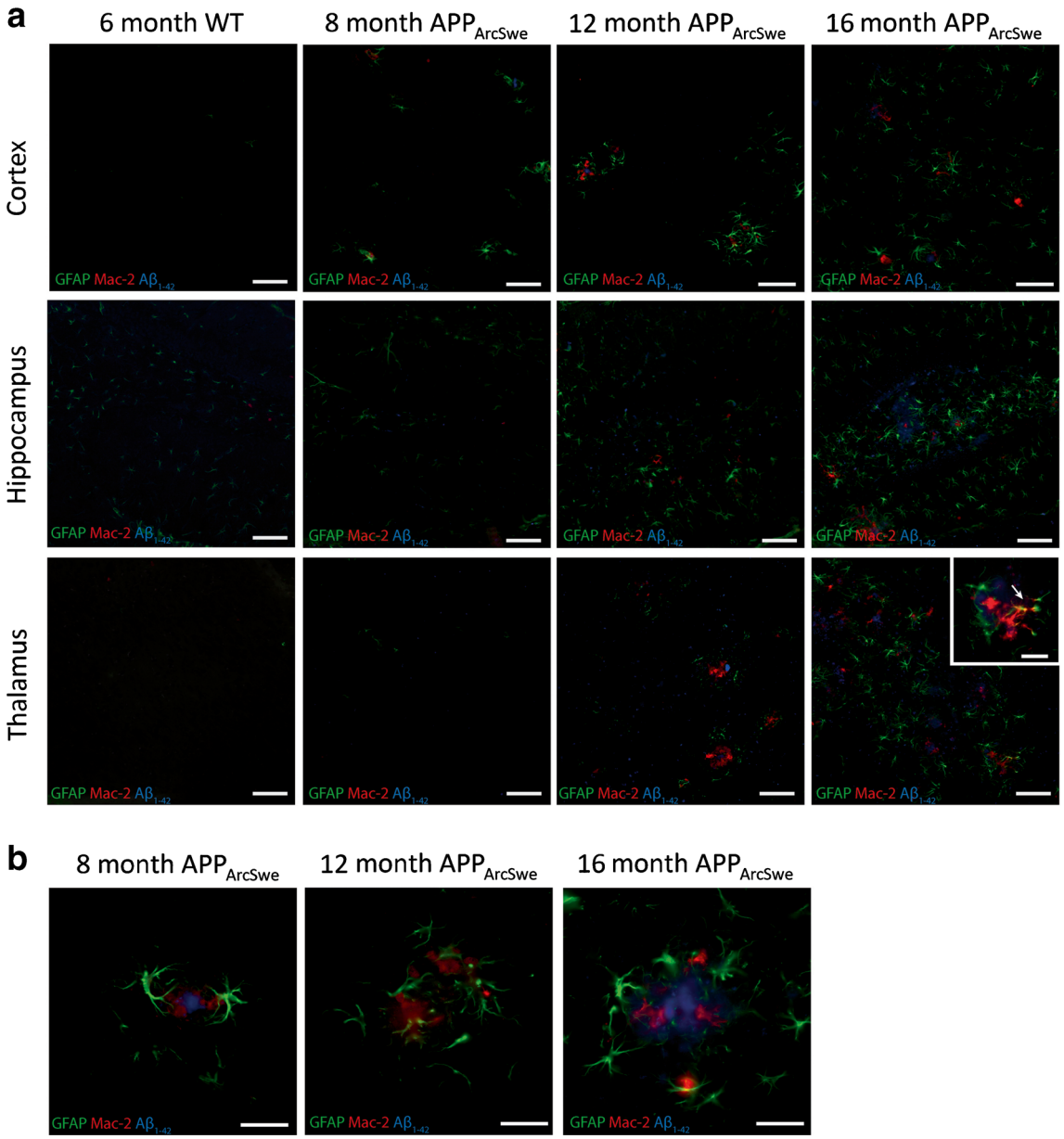

Fig. 3 Visualization of reactive astrocytes and microglia in brains isolated from 8- to 16-month-old mice. In all images, astrocytes are detected in green by anti-GFAP (Sigma Aldrich, G3893), microglia are detected in red by anti-Mac-2 (Cedarlane, CL8942AP), and Aβ is detected in blue by anti-Aβ42 (Life Technologies, 700,254). **a** Images of GFAP-, Mac-2-, and Aβ42-stained brains from $APP_{Arc\text{-}Swe}$ and WT mice of different ages. Horizontal rows show the expression in cortex, hippocampus, and thalamus. White arrow (inset) indicates double-labeled cells. All images were taken at ×20 except for the inserted images that were taken with ×63 oil immersion objective. Scale bars represent 50 μm (20 μm in inserted images). **b** Images of GFAP-, Mac-2-, and Aβ42-stained brains from 8- to 16-month $APP_{Arc\text{-}Swe}$ mice in cortex in the vicinity of aggregated Aβ; higher magnification than in (**a**). All images were taken with ×63 oil immersion objective. Scale bars represent 20 μm.

reported elevated [^{11}C]DED binding in APP_{swe} mice compared with WT mice [30]. Somewhat contradictory to the present study, this previous study showed higher [^{11}C]DED binding in young 6-month-old APP_{swe} mice compared with older mice. This decline in [^{11}C]DED binding between 6-month-old APP_{swe} mice and older mice could, however, not be confirmed by *in vitro* autoradiography [30]. One limitation of the present [^{11}C]DED data is the low number of animals in each group, and that animals younger than 8 months were not investigated with PET.

During AD, an elevation of GFAP-positive cells has been shown in the brain in parallel with the progression of Braak stages [31]. Vimentin is rarely expressed in astrocytes in the mature, healthy brain, and only by precursor cells in regions where neurogenesis occurs. However, in reactive astrocytes, activated as a result of, for example, a brain insult, vimentin

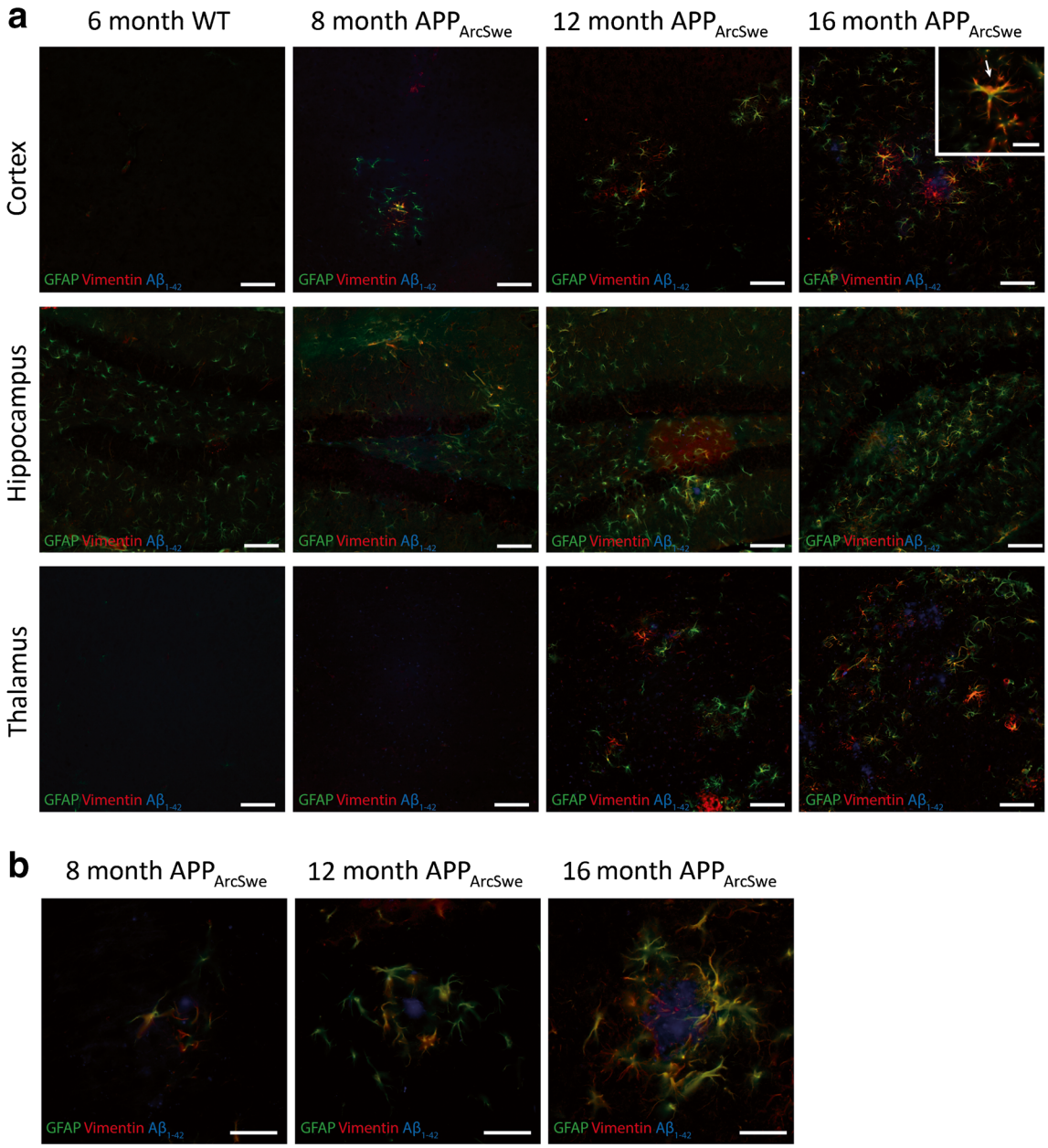

Fig. 4 Visualization of reactive astrocytes in brains isolated from 8 -to 16-month mice. In all images, astrocytes are detected in green by anti-GFAP (Sigma Aldrich, G3893) and in red by anti-vimentin (Millipore, AB5733), and amyloid plaques are detected in blue by anti-Aβ42 (Life Technologies, 700,254). **a** Images of GFAP-, vimentin-, and Aβ42-stained brains from APP$_{Arc-Swe}$ and WT mice of different ages. Horizontal panels show the expression in cortex, hippocampus, and thalamus. White arrows (inset) indicate examples of double-labeled cells. All images were taken at 20× except for the inserted images that were taken with 63× oil immersion objective. Scale bars represent 50 μm (20 μm in inserted images). **b** Images of GFAP-, vimentin-, and Aβ42-stained brains from 8- to 16-month APP$_{Arc-Swe}$ mice in the cortex in the vicinity of aggregated Aβ; higher magnification than in (**a**). All images were taken with ×63 oil immersion objective. Scale bars represent 20 μm.

expression is intensively upregulated in astrocytes in the damaged regions. GFAP expression is in addition to the damaged area also diffusely observed in the rest of the brain [41]. In the present study, we found that opposite to [^{11}C]DED binding, GFAP and vimentin increased with Aβ pathology. MAO-B showed very limited co-localization with GFAP. The biochemical quantification of GFAP with ELISA confirmed the results obtained with immunohistochemistry and indicated that increased GFAP levels were a consequence of, or at least mirrored, the Aβ accumulation. These results are also supported by the previous studies in APP$_{swe}$ mice and on *post mortem* human brain tissue [30, 42]. Another preclinical study, conducted in APP/PS1 mice, focusing on GABA function reported low degree of co-

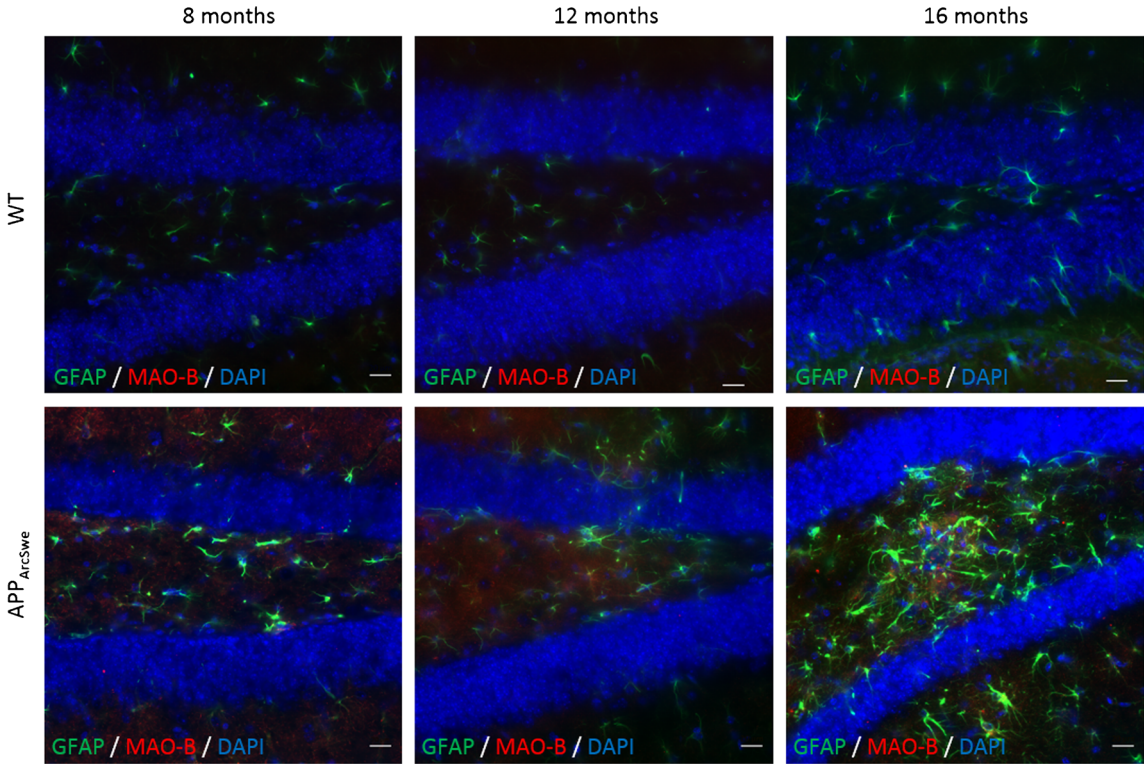

Fig. 5 Lack of co-localization between GFAP and MAO-B in hippocampus. Astrocytes are detected in green by anti-GFAP (Sigma Aldrich, G3893) and in red by anti-MAO-B (Sigma Aldrich, HPA002328). All images were taken at ×40. Scale bars represent 20 μm.

localization of MAO-B and GFAP [43]. Thus, it appears that MAO-B and GFAP/vimentin could be markers for different stages of astrogliosis, or different types of astrocytes, or even completely different cell types, where MAO-B levels remain stable while GFAP/vimentin expression increase during Aβ accumulation.

Another PET-imaging target related to neuroinflammation is the mitochondrial translocator protein (TSPO). TSPO

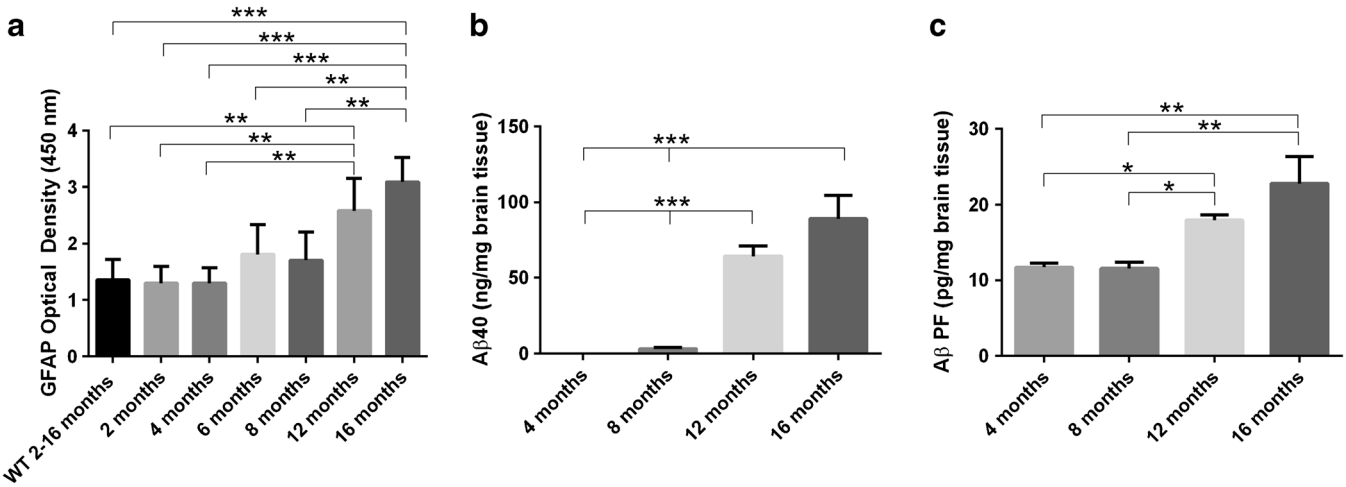

Fig. 6 **a** Biochemical analysis of GFAP and Aβ in brain tissue. GFAP levels in young APP_{ArcSwe} mice were low and comparable with WT mice of all ages. GFAP levels in APP_{ArcSwe} mice were then increased from the age of 6–8 months. **b** Total Aβ levels started to increase in APP_{ArcSwe} at 8 months and were further increased at 16 months. **c** Aβ protofibril levels in APP_{ArcSwe} could be detected already at 4 months and increased further at 12 and 16 months. (n = 4 APP_{ArcSwe}, n = 2 WT per age group in (**a**), and n = 5 per age group in (**b**) and (**c**)).

is known to be upregulated in reactive microglia. Studies in mouse models of Aβ pathology have shown that binding of TSPO PET radioligand [^{11}C]PBR28 was elevated in 6-month-old 5× FAD transgenic mice compared with WT controls [44], while another TSPO ligand, [^{11}C]PK11195, displayed an age-dependent increase in binding in 13–19-month-old APP_{Swe}/$PSEN1_{DeltaE9}$ mice [45]. Thus, TSPO imaging, in line with GFAP/vimentin, reflected level of Aβ accumulation.

As of today, a number PET studies has been performed with [^{11}C]DED in human AD patients [26–29, 46, 47]. The majority of the published results show that the binding of [^{11}C]DED is increased in AD patients compared with healthy age-matched controls. Interestingly, it has been reported that the increase may be highest in MCI and prodromal AD indicating that astrogliosis measured by [^{11}C]DED is occurring early in the human AD brain [26, 27, 29]. Thus, the clinical studies are in line with the results obtained in the APP_{ArcSwe} mice in the present study.

The intrabrain accumulation of monomeric Aβ and the formation of Aβ oligomers and protofibrils are likely to precede the formation of dense core plaques. We hypothesize that the increase in MAO-B levels may be a consequence of these soluble Aβ species, which may be engulfed by astrocytes [20] and potentially be able to interact with MAO-B at the mitochondria. This hypothesis is also supported by earlier experiments in cell cultures showing that Aβ 25–35 peptide induces expression of MAO-B in cultured rat astrocytes [48].

Conclusions

PET imaging with [^{11}C]DED is therefore a useful tool to diagnose neuroinflammation at an early stage in AD. When analyzing changes in [^{11}C]DED binding, including a decline in binding as has been reported in some clinical studies when patients have progressed from MCI/prodromal AD to AD, it is important to consider that such decline may not reflect a decline in astrogliosis *per se*. Different subclasses of astrocytes may express different proteins as a response to activation. The present study showed that changes in MAO-B levels and GFAP/vimentin did not occur simultaneously and did not co-localize to the same cell population. Thus, a single marker such as MAO-B, GFAP, or vimentin, may not be enough for estimation of the total level of astrogliosis.

Acknowledgements. The authors acknowledge R.K. Selvaraju, S. Estrada, and V. Asplund at the Preclinical PET Platform, Uppsala University, Sweden, for excellent technical assistance with PET scanning and to Liza Al-Zaibari and Silvio R. Meier for assistance with the biochemical measurements of Aβ and GFAP.

Funding This work was supported by Alzheimerfonden, Hjärnfonden, Åhlén-stiftelsen, Stohnes stiftelse, and Uppsala Berzelii Technology Centre for Neurodiagnostics.

Compliance with Ethical Standards. All mice used in this study were maintained under protocols approved by the Uppsala County Animal Ethics board, and followed the rules and regulations of the Swedish Animal Welfare Agency (approval number C17/14).

Conflict of Interest

The authors declare that they have no conflict of interest.

References

1. Hardy JA, Higgins GA (1992) Alzheimer's disease: the amyloid cascade hypothesis. Science 256(5054):184–185. https://doi.org/10.1126/science.1566067
2. Hartley DM, Walsh DM, Ye CP, Diehl T, Vasquez S, Vassilev PM, Teplow DB, Selkoe DJ (1999) Protofibrillar intermediates of amyloid beta-protein induce acute electrophysiological changes and progressive neurotoxicity in cortical neurons. J Neurosci 19(20):8876–8884
3. Klyubin I, Walsh DM, Cullen WK, Fadeeva JV, Anwyl R, Selkoe DJ, Rowan MJ (2004) Soluble Arctic amyloid beta protein inhibits hippocampal long-term potentiation in vivo. Eur J Neurosci 19(10):2839–2846. https://doi.org/10.1111/j.1460-9568.2004.03389.x
4. Klyubin I, Cullen WK, NW H, Rowan MJ (2012) Alzheimer's disease Abeta assemblies mediating rapid disruption of synaptic plasticity and memory. Mol Brain 5(1):25. https://doi.org/10.1186/1756-6606-5-25
5. Walsh DM, Klyubin I, Fadeeva JV, Cullen WK, Anwyl R, Wolfe MS, Rowan MJ, Selkoe DJ (2002) Naturally secreted oligomers of amyloid beta protein potently inhibit hippocampal long-term potentiation in vivo. Nature 416(6880):535–539. https://doi.org/10.1038/416535a
6. Lacor PN, Buniel MC, Furlow PW, Sanz Clemente A, Velasco PT, Wood M, Viola KL, Klein WL (2007) Abeta oligomer-induced aberrations in synapse composition, shape, and density provide a molecular basis for loss of connectivity in Alzheimer's disease. J Neurosci 27(4):796–807. https://doi.org/10.1523/JNEUROSCI.3501-06.2007
7. Esparza TJ, Zhao H, Cirrito JR, Cairns NJ, Bateman RJ, Holtzman DM, Brody DL (2013) Amyloid-beta oligomerization in Alzheimer dementia versus high-pathology controls. Ann Neurol 73(1):104–119. https://doi.org/10.1002/ana.23748
8. Obulesu M, Jhansilakshmi M (2014) Neuroinflammation in Alzheimer's disease: an understanding of physiology and pathology. Int J Neurosci 124(4):227–235. https://doi.org/10.3109/00207454.2013.831852
9. Bagyinszky E, Youn YC, An SSA, Kim S (2014) Characterization of inflammatory biomarkers and candidates for diagnos. BioChip Journal 8(3):155–162. https://doi.org/10.1007/s13206-014-8301-1
10. Eroglu C, Barres BA (2010) Regulation of synaptic connectivity by glia. Nature 468(7321):223–231. https://doi.org/10.1038/nature09612
11. Sofroniew MV, Vinters HV (2010) Astrocytes: biology and pathology. Acta Neuropathol 119(1):7–35. https://doi.org/10.1007/s00401-009-0619-8
12. Verkhratsky A, Nedergaard M, Hertz L (2015) Why are astrocytes important? Neurochem Res 40(2):389–401. https://doi.org/10.1007/s11064-014-1403-2
13. Pekny M, Wilhelmsson U, Pekna M (2014) The dual role of astrocyte activation and reactive gliosis. Neurosci Lett 565:30–38. https://doi.org/10.1016/j.neulet.2013.12.071
14. Osborn LM, Kamphuis W, Wadman WJ, Hol EM (2016) Astrogliosis: an integral player in the pathogenesis of Alzheimer's disease. Prog Neurobiol 144:121–141. https://doi.org/10.1016/j.pneurobio.2016.01.001
15. Cai Z, Hussain MD, Yan LJ (2014) Microglia, neuroinflammation, and beta-amyloid protein in Alzheimer's disease. Int J Neurosci 124(5):307–321. https://doi.org/10.3109/00207454.2013.833510
16. Sastre M, Klockgether T, Heneka MT (2006) Contribution of inflammatory processes to Alzheimer's disease: molecular mechanisms. Int J Dev Neurosci 24(2-3):167–176. https://doi.org/10.1016/j.ijdevneu.2005.11.014

17. Breunig JJ, Guillot-Sestier MV, Town T (2013) Brain injury, neuroinflammation and Alzheimer's disease. Front Aging Neurosci 5:26
18. Loov C, Hillered L, Ebendal T, Erlandsson A (2012) Engulfing astrocytes protect neurons from contact-induced apoptosis following injury. PLoS One 7(3):e33090. https://doi.org/10.1371/journal.pone.0033090
19. Jones RS, Minogue AM, Connor TJ, Lynch MA (2013) Amyloid-beta-induced astrocytic phagocytosis is mediated by CD36, CD47 and RAGE. J NeuroImmune Pharmacol 8(1):301–311. https://doi.org/10.1007/s11481-012-9427-3
20. Sollvander S, Nikitidou E, Brolin R et al (2016) Accumulation of amyloid-beta by astrocytes result in enlarged endosomes and microvesicle-induced apoptosis of neurons. Mol Neurodegener 11(1):38. https://doi.org/10.1186/s13024-016-0098-z
21. Lindstrom V, Gustafsson G, Sanders LH et al (2017) Extensive uptake of alpha-synuclein oligomers in astrocytes results in sustained intracellular deposits and mitochondrial damage. Mol Cell Neurosci 82:143–156. https://doi.org/10.1016/j.mcn.2017.04.009
22. Nielsen HM, Mulder SD, Belien JA et al (2010) Astrocytic A beta 1-42 uptake is determined by a beta-aggregation state and the presence of amyloid-associated proteins. Glia 58(10):1235–1246. https://doi.org/10.1002/glia.21004
23. Saura J, Bleuel Z, Ulrich J, Mendelowitsch A, Chen K, Shih JC, Malherbe P, da Prada M, Richards JG (1996) Molecular neuroanatomy of human monoamine oxidases A and B revealed by quantitative enzyme radioautography and in situ hybridization histochemistry. Neuroscience 70(3):755–774. https://doi.org/10.1016/S0306-4522(96)83013-2
24. Fowler JS, MacGregor RR, Wolf AP et al (1987) Mapping human brain monoamine oxidase a and B with 11C-labeled suicide inactivators and PET. Science 235(4787):481–485. https://doi.org/10.1126/science.3099392
25. Gulyas B, Pavlova E, Kasa P et al (2011) Activated MAO-B in the brain of Alzheimer patients, demonstrated by [11C]-L-deprenyl using whole hemisphere autoradiography. Neurochem Int 58(1):60–68. https://doi.org/10.1016/j.neuint.2010.10.013
26. Choo IL, Carter SF, Scholl ML, Nordberg A (2014) Astrocytosis measured by (1)(1)C-deprenyl PET correlates with decrease in gray matter density in the parahippocampus of prodromal Alzheimer's patients. Eur J Nucl Med Mol Imaging 41(11):2120–2126. https://doi.org/10.1007/s00259-014-2859-7
27. Carter SF, Scholl M, Almkvist O, Wall A, Engler H, Langstrom B, Nordberg A (2012) Evidence for astrocytosis in prodromal Alzheimer disease provided by 11C-deuterium-L-deprenyl: a multitracer PET paradigm combining 11C-Pittsburgh compound B and 18F-FDG. J Nucl Med 53(1):37–46. https://doi.org/10.2967/jnumed.110.087031
28. Rodriguez-Vieitez E, Carter SF, Chiotis K, Saint-Aubert L, Leuzy A, Scholl M, Almkvist O, Wall A, Langstrom B, Nordberg A (2016) Comparison of early-phase 11C-deuterium-l-deprenyl and 11C-Pittsburgh compound B PET for assessing brain perfusion in Alzheimer disease. J Nucl Med 57(7):1071–1077. https://doi.org/10.2967/jnumed.115.168732
29. Rodriguez-Vieitez E, Saint-Aubert L, Carter SF, Almkvist O, Farid K, Schöll M, Chiotis K, Thordardottir S, Graff C, Wall A, Långström B, Nordberg A (2016) Diverging longitudinal changes in astrocytosis and amyloid PET in autosomal dominant Alzheimer's disease. Brain 139(3):922–936. https://doi.org/10.1093/brain/awv404
30. Rodriguez-Vieitez E, Ni R, Gulyas B et al (2015) Astrocytosis precedes amyloid plaque deposition in Alzheimer APPswe transgenic mouse brain: a correlative positron emission tomography and in vitro imaging study. Eur J Nucl Med Mol Imaging 42(7):1119–1132. https://doi.org/10.1007/s00259-015-3047-0
31. Simpson JE, Ince PG, Lace G, Forster G, Shaw PJ, Matthews F, Savva G, Brayne C, Wharton SB, MRC Cognitive Function and Ageing Neuropathology Study Group (2010) Astrocyte phenotype in relation to Alzheimer-type pathology in the ageing brain. Neurobiol Aging 31(4):578–590. https://doi.org/10.1016/j.neurobiolaging.2008.05.015
32. Philipson O, Lord A, Gumucio A, O'Callaghan P, Lannfelt L, Nilsson LNG (2010) Animal models of amyloid-beta-related pathologies in Alzheimer's disease. FEBS J 277(6):1389–1409. https://doi.org/10.1111/j.1742-4658.2010.07564.x
33. Lord A, Kalimo H, Eckman C, Zhang XQ, Lannfelt L, Nilsson LNG (2006) The Arctic Alzheimer mutation facilitates early intraneuronal Abeta aggregation and senile plaque formation in transgenic mice. Neurobiol Aging 27(1):67–77. https://doi.org/10.1016/j.neurobiolaging.2004.12.007
34. Sehlin D, Fang XT, Cato L, Antoni G, Lannfelt L, Syvänen S (2016) Antibody-based PET imaging of amyloid beta in mouse models of Alzheimer's disease. Nat Commun 7:10759. https://doi.org/10.1038/ncomms10759
35. Kumlien E, Bergstrom M, Lilja A, Andersson J, Szekeres V, Westerberg CE, Westerberg G, Antoni G, Langstrom B (1995) Positron emission tomography with [11C]deuterium-deprenyl in temporal lobe epilepsy. Epilepsia 36(7):712–721. https://doi.org/10.1111/j.1528-1157.1995.tb01051.x
36. Loening AM, Gambhir SS (2003) AMIDE: a free software tool for multimodality medical image analysis. Mol Imaging 2(3):131–137. https://doi.org/10.1162/153535003322556877
37. Ma Y, Hof PR, Grant SC, Blackband SJ, Bennett R, Slatest L, McGuigan MD, Benveniste H (2005) A three-dimensional digital atlas database of the adult C57BL/6J mouse brain by magnetic resonance microscopy. Neuroscience 135(4):1203–1215. https://doi.org/10.1016/j.neuroscience.2005.07.014
38. Lammertsma AA, Hume SP (1996) Simplified reference tissue model for PET receptor studies. NeuroImage 4(3):153–158. https://doi.org/10.1006/nimg.1996.0066
39. Sehlin D, Englund H, Simu B, Karlsson M, Ingelsson M, Nikolajeff F, Lannfelt L, Pettersson FE (2012) Large aggregates are the major soluble Abeta species in AD brain fractionated with density gradient ultracentrifugation. PLoS One 7(2):e32014. https://doi.org/10.1371/journal.pone.0032014
40. Magnusson K, Sehlin D, Syvanen S et al (2013) Specific uptake of an amyloid-beta protofibril-binding antibody-tracer in AbetaPP transgenic mouse brain. J Alzheimers Dis 37(1):29–40. https://doi.org/10.3233/JAD-130029
41. Petito CK, Morgello S, Felix JC, Lesser ML (1990) The two patterns of reactive astrocytosis in postischemic rat brain. J Cereb Blood Flow Metab 10(6):850–859. https://doi.org/10.1038/jcbfm.1990.141
42. Marutle A, Gillberg PG, Bergfors A et al (2013) (3)H-deprenyl and (3)H-PIB autoradiography show different laminar distributions of astroglia and fibrillar beta-amyloid in Alzheimer brain. J Neuroinflammation 10:90
43. Jo S, Yarishkin O, Hwang YJ, Chun YE, Park M, Woo DH, Bae JY, Kim T, Lee J, Chun H, Park HJ, Lee DY, Hong J, Kim HY, Oh SJ, Park SJ, Lee H, Yoon BE, Kim YS, Jeong Y, Shim I, Bae YC, Cho J, Kowall NW, Ryu H, Hwang E, Kim D, Lee CJ (2014) GABA from reactive astrocytes impairs memory in mouse models of Alzheimer's disease. Nat Med 20(8):886–896. https://doi.org/10.1038/nm.3639
44. Mirzaei N, Tang SP, Ashworth S, Coello C, Plisson C, Passchier J, Selvaraj V, Tyacke RJ, Nutt DJ, Sastre M (2016) In vivo imaging of microglial activation by positron emission tomography with [(11)C]PBR28 in the 5XFAD model of Alzheimer's disease. Glia 64(6):993–1006. https://doi.org/10.1002/glia.22978
45. Venneti S, Lopresti BJ, Wang G, Hamilton RL, Mathis CA, Klunk WE, Apte UM, Wiley CA (2009) PK11195 labels activated microglia in Alzheimer's disease and in vivo in a mouse model using PET. Neurobiol Aging 30(8):1217–1226. https://doi.org/10.1016/j.neurobiolaging.2007.11.005
46. Hirvonen J, Kailajarvi M, Haltia T et al (2009) Assessment of MAO-B occupancy in the brain with PET and [11C]-L-deprenyl-D2: a dose-finding study with a novel MAO-B inhibitor. Clin Pharmacol Ther 85(5):506–512. https://doi.org/10.1038/clpt.2008.241
47. Santillo AF, Gambini JP, Lannfelt L, Långström B, Ulla-Marja L, Kilander L, Engler H (2011) In vivo imaging of astrocytosis in Alzheimer's disease: an (1)(1)C-L-deuteriodeprenyl and PIB PET study. Eur J Nucl Med Mol Imaging 38(12):2202–2208. https://doi.org/10.1007/s00259-011-1895-9
48. Song W, Zhou LJ, Zheng SX, Zhu XZ (2000) Amyloid-beta 25-35 peptide induces expression of monoamine oxidase B in cultured rat astrocytes. Acta Pharmacol Sin 21(6):557–563